**Supporting information**

**Chemical Design and Synthesis of Superior Single-Atom Electrocatalysts *via* In-Situ Polymerization**

Haomin Xu,[a,b] Shibo Xi,[c] Jing Li,[b] Shikai Liu,[d] Pin Lyu,[a] Wei Yu,[a] Tao Sun,[a] Dong-Chen Qi,[e] Qian He,[d] Hai Xiao,[f] Ming Lin,[g] Jishan Wu,*[,a] Jia Zhang*[,h] and Jiong Lu*[,a,b]

[a] Department of Chemistry, National University of Singapore, Singapore 117543

[b] Centre for Advanced 2D Materials and Graphene Research Centre, National University of Singapore, Singapore 117546

[c] Institute of Chemical and Engineering Sciences, Singapore 627833

[d] Department of Materials Science & Engineering, National University of Singapore, Singapore 117575

[e] Centre for Materials Science, School of Chemistry and Physics, Queensland University of Technology, QLD 4001, Australia

[f] Department of Chemistry, Tsinghua University, Beijing 100084, China

[g] Institute of Materials Research and Engineering, Agency for Science, Technology and Research (A*STAR), Singapore 138634

[h] Institute of High Performance Computing, Agency for Science, Technology and Research (A*STAR), Singapore 138632

**AUTHOR INFORMATION**

Corresponding Authors

* chmwuj@nus.edu.sg
* zhangj@ihpc.a-star.edu.sg
* chmluj@nus.edu.sg

**Experimental Section**

**Materials and Chemicals**

Unless otherwise noted, materials obtained from commercial suppliers were used without further purification.

**Material Synthesis**

**Synthesis of iron(II) tetranitrophthalocyanine (FePc(NO$_2$)$_4$)**

A mixture of 4-nitrophthalonitrile (5.7 g), iron(II) chloride tetrahydrate (1.5 g), urea (14.4g) and ammonium molybdate (75 mg) were finely ground and placed in a 100 mL round-bottom flask. The mixture was continually stirred at 160 °C for 5 h under N$_2$ atmosphere. After cooling to ambient temperature, the r0065sulting product was stirred in an aqueous HCl solution (1 M, 450 mL) and aqueous KOH solution (1 M, 450 mL) at 90 °C for 1 h, respectively. This process was repeated again. The residue was then dissolved in DMF and filtered. The solvent in filtrate was removed under reduced pressure to obtain FePc(NO$_2$)$_4$.

**Synthesis of amino group functionalized iron phthalocyanine (NH$_2$-FePc)**

FePc(NO$_2$)$_4$ (3.0 g) was converted to NH$_2$-FePc by reacting with sodium sulfide nonahydrate (11.5 g) in DMF (60 mL) at 60 °C for 1 h under N$_2$ atmosphere. The solution was then poured into water (150 mL), and the precipitate was collected by centrifugation, repeatedly washed with water until neutral pH is obtained. The product was dried under vacuum and stored under N$_2$ atmosphere.

**Synthesis of polymerized FePc (p-FePc)**

A Schlenk tube containing NH$_2$-FePc (20 mg) was evacuated and then refilled with N$_2$. To the tube, a dry and degassed DMSO (90 mL) was added. To the solution, a solution of DDQ (120 mg) and TFA (0.4 mL) in dry and degassed DMSO (10 mL) was added, and the solution was stirred at 100 °C for 5 h. The solution was then poured into ethanol (100 mL), and the p-FePc was collected by centrifugation, repeatedly washed three times with ethanol. The product was dried under vacuum.

**Synthesis of p-FePc/CNTs**

CNTs were purified according to reported method.[1] A Schlenk tube containing purified CNTs (50 mg) and NH$_2$-FePc (10 mg) was evacuated and then refilled with N$_2$. To the tube, a dry and degassed DMSO (45 mL) was added. The solution was sonicated for 30 min and stirred at ambient temperature for 30 min. To the solution, a solution of DDQ (60 mg) and TFA (0.2 mL) in dry and degassed DMSO (5 mL) was added, and the mixture was stirred at 100 °C for 5 h. The p-FePc/CNTs was collected by centrifugation and washed three times with DMSO and three times with ethanol. The product was dried under vacuum. A series of p-FePc/CNTs samples with different Fe contents were also prepared, including 0.38 wt%, 0.65 wt%, 0.81 wt%, 0.89 wt% and 1.98 wt%, from the monomer (NH$_2$-FePc) and CNTs with a weight ratio of 1:10, 1:8, 1:6, 1:5 and 2:5, respectively.

**Synthesis of FePc/CNTs**

A DMF solution (50 mL) of purified CNTs (50 mg) and FePc (5.3 mg) was sonicated for 30 min and stirred at ambient temperature for 12 h. The FePc/CNTs was collected by centrifugation and washed three times with DMF and three times with ethanol. The product was dried under vacuum.

**Synthesis of NH$_2$-FePc/CNTs**

A DMF solution (50 mL) of purified CNTs (50 mg) and NH$_2$-FePc (4.1 mg) was sonicated for 30 min and stirred at ambient temperature for 12 h. The FePc/CNTs was collected by centrifugation and washed three times with DMF and three times with ethanol. The product was dried under vacuum.

**Synthesis of p-FePc+CNTs mixture**

A DMSO solution (50 mL) of purified CNTs (50 mg) and p-FePc (10 mg) was sonicated for 30 min and stirred at ambient temperature for 12 h. The mixture was collected and washed with the same method used in the synthesis of p-FePc.

**Materials Characterization**

SEM images were taken on a FEI Verios 460 Field Emission microscopy operated at 2 kV and 100 pA. TEM images were obtained with a FEI Titan 80-300 operated at 200 kV. HAADF-STEM images were obtained with a JEOL ARM200CF S/TEM operated at 200 kV, equipped with an Oxford Instrument X-ray energy dispersive spectrometer. AFM images were taken on a Bruker Multimode 8 and Dimension FastScan. All FT-IR spectra were recorded on a Bruker vertex 80v spectrometer under vacuum. XPS (Omicron EAC2000-125) measurements were conducted using Al Kα radiation (hν = 1486.6 eV). The Fe loadings in all the samples were measured by an inductively coupled plasma atomic emission spectrometer (ICP-AES); therein all samples were dissolved in hot fresh aqua regia. Thermogravimetric analysis (TGA) was carried out on a Discovery TGA Thermogravimetric Analyzer (TA Instruments) with a heating rate of 10 °C min$^{-1}$ in air. N K-edge NEXAFS measurements were performed in partial electron yield mode at the ultrahigh vacuum endstation of Soft X-ray Spectroscopy beamline at the Australian Synchrotron. Photon energy calibration was done using spectra taken from previously calibrated stable reference foils measured in parallel with the data. The XANES and the EXAFS measurements of Fe K-edge were carried out at the XAFCA beamline of the Singapore Synchrotron Light Source (SSLS).[2] A Si (111) double-crystal monochromator was applied to filter the X-ray beam. Fe foils were used for the energy calibration, and all samples were measured under transmission mode at room temperature. The EXAFS oscillations χ(k) were extracted and analyzed using the Demeter software package.[3]

**Electrochemical measurements**

All of the measurements were carried out using a CHI 760E electrochemical workstation with a standard three-electrode setup. 2 mg of catalyst and 6 μl of 5 wt% Nafion solution were dispersed in 0.5 ml of ethanol by at least 30 min sonication to form a homogeneous ink. Then 10 μl of the catalyst ink (containing 40 μg of catalyst) was loaded onto a glassy carbon rotating disk electrode of 5 mm in diameter (Pine Instruments) (note the loading of catalysts is determined to be 0.2 mg cm$^{-2}$). For 20 wt% Pt/C catalyst, the loading on glassy carbon rotating disk electrode is determined to be 0.1 mg cm$^{-2}$. This sample modified glassy carbon electrode was used as working electrode, and a saturated calomel electrode and a graphite rod were used as the reference electrode and the counter electrode, respectively. Prior to the measurement, the 0.1 M KOH electrolyte was saturated with N$_2$/O$_2$ by bubbling the corresponding gas for 30 min. For the CV measurements, the working electrode was cycled at least 20 times before data were recorded at a scan rate of 5 mV s$^{-1}$. The electrochemical impedance spectroscopy of p-FePc/CNTs and p-FePc was measured in the frequency range from 10$^5$

to 0.01 Hz at 0.90 V vs. RHE. For the RDE measurement, the working electrode was scanned cathodically at a rate of 5 mV s$^{-1}$ with varying rotating speed from 400 rpm to 1600 rpm. Koutecky–Levich plots were analyzed at various electrode potentials. The slopes of their best linear fit lines were used to calculate the electron transfer number on the basis of the Koutecky-Levich equation.[4] For the Tafel plot, the kinetic current was calculated from the mass-transport correction of RDE by:

$$J_K = \frac{J \times J_L}{J_L - J}$$

where $J$ is measured current density, $J_K$ and $J_L$ are kinetic- and diffusion-limiting current densities. For the RRDE measurements, catalyst inks and electrodes were prepared by the same method as RDE's. Then 12.5 μl of the catalyst ink (containing 50 μg of catalyst) was loaded onto a rotating ring-disk electrode of 5.61 mm in disk diameter (Pine Instruments) (note the loading of the catalysts is determined to be 0.2 mg cm$^{-2}$). The disk electrode was scanned cathodically at a rate of 5 mV s$^{-1}$ and the ring potential was constant at 1.4 V vs. RHE. The peroxide yield (%HO$_2^-$) and the electron transfer number (n) were determined by the followed equations:

$$\%HO_2{}^- = 200 \times \frac{I_R/N}{(I_R/N) + I_D}$$

$$n = 4 \times \frac{I_D}{(I_R/N) + I_D}$$

where $I_D$ is disk current, $I_R$ is ring current and $N = 0.37$ is current collection efficiency of the Pt ring. The electrochemical double-layer capacitance (C$_{dl}$) of the catalysts was measured using the cyclic voltammogram at different scan rates in a small potential range (1.1-1.2 V vs. RHE) without faradaic processes. Electrochemical surface area (ECSA) was calculated as below:

$$ECSA = \frac{C_{dl}}{C_{Ref}}$$

where C$_{dl}$ is the electrochemical double-layer capacitance of the catalyst, C$_{Ref}$ is the double-layer capacitance of a flat surface, and the CRef value is adopted as 0.04 mF cm$^{-2}$.[5,6] TOF is calculated using the equation below[7,8]:

$$TOF = \frac{I_{measured}/F}{M_{catalyst} \times Fe\%/M_{Fe}}$$

where $I_{measured}$ is the measured current, $F$ is Faraday constant, $M_{catalyst}$ is the mass of catalyst on the electrode, $Fe\%$ is the Fe content in the catalyst, $M_{Fe}$ is the molar mass of Fe (55.8 g mol$^{-1}$).

**Zn-oxygen batteries**

The primary Zn-oxygen batteries were measured in a home-made electrochemical cell with two-electrode configuration. p-FePc/CNTs or Pt/C catalyst loaded on carbon fiber paper (Toray 060, 0.5 cm$^2$, catalyst loading 1mg cm$^{-2}$) was used as a gas diffusion electrode for cathode, and a Zn foil and 6 M KOH were used as anode and electrolyte. During measurements, oxygen gas was continuously supplied to the backside of cathode. The discharge polarization curves were obtained via linear sweep voltammetry at the scan rate of 10 mV s$^{-1}$. To compare the catalytic performance of different catalysts

on the same bias, the internal resistance was corrected to R = 1 Ω for consistency throughout the experiment.[9-11]

**Computational Method**

DFT calculations were performed using the Vienna Ab initio Simulation package (VASP)[12,13] in which a plane-wave basis set was used. The electron-ion interaction was modelled using the projector augmented wave (PAW) method.[14,15] The spin-polarized general gradient approximation (GGA) scheme with the PBE form was used for the exchange and correlation functional.[16] The plane-wave cutoff energy was set to 450 eV. To describe the 2D network structure after polymerization, a periodic model was built for p-FePc, where periodic boundary conditions were employed along x and y directions (15.39 Å x 15.39 Å) with a vacuum region of 13 Å along z direction. In addition, a cluster model was chosen to simulate FePc molecule. A 2×2×1 k-point mesh was used for the periodic system and a Gamma point was applied to the cluster model, respectively.

In this work, Gibbs free energies of adsorbed intermediates are calculated by $G = E + ZPE + E_{int} - TS - neU$, where E is the total energy from DFT calculation. The zero-point energy (ZPE), internal energy contribution ($E_{int}$) and entropic contribution (S) to the free energy were calculated according to the reference.[17] For gaseous molecules, the corresponding zero-point and thermal corrections to Gibbs free energy were obtained with the Gaussian 09 Program,[18] where all calculations were performed at B3LYP/6-31G* level.[19,20] The binding energy of the intermediate *O is defined as $E_{b,*O} = E_{*O} - E_* - (E_{H_2O} - E_{H_2})$, where $E_{*O}$, $E_*$, $E_{H_2O}$ and $E_{H_2}$ represents the total energy of the O-adsorbed FePc/p-FePc, clean FePc/p-FePc, gas phase $H_2O$ and gas phase $O_2$, respectively.[21] In addition, the crystal orbital Hamilton Population (COHP) of Fe-O bond was calculated by LOBSTER (version 2.2.1).[22-25]
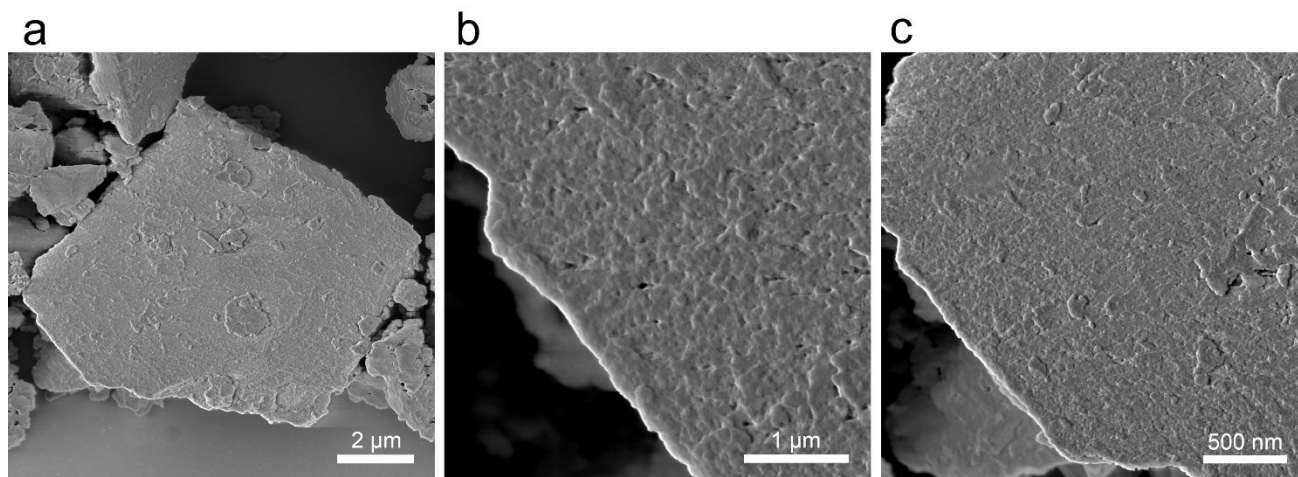
**Figure S1.** (a-c) Large-area and magnified SEM images of p-FePc flakes.
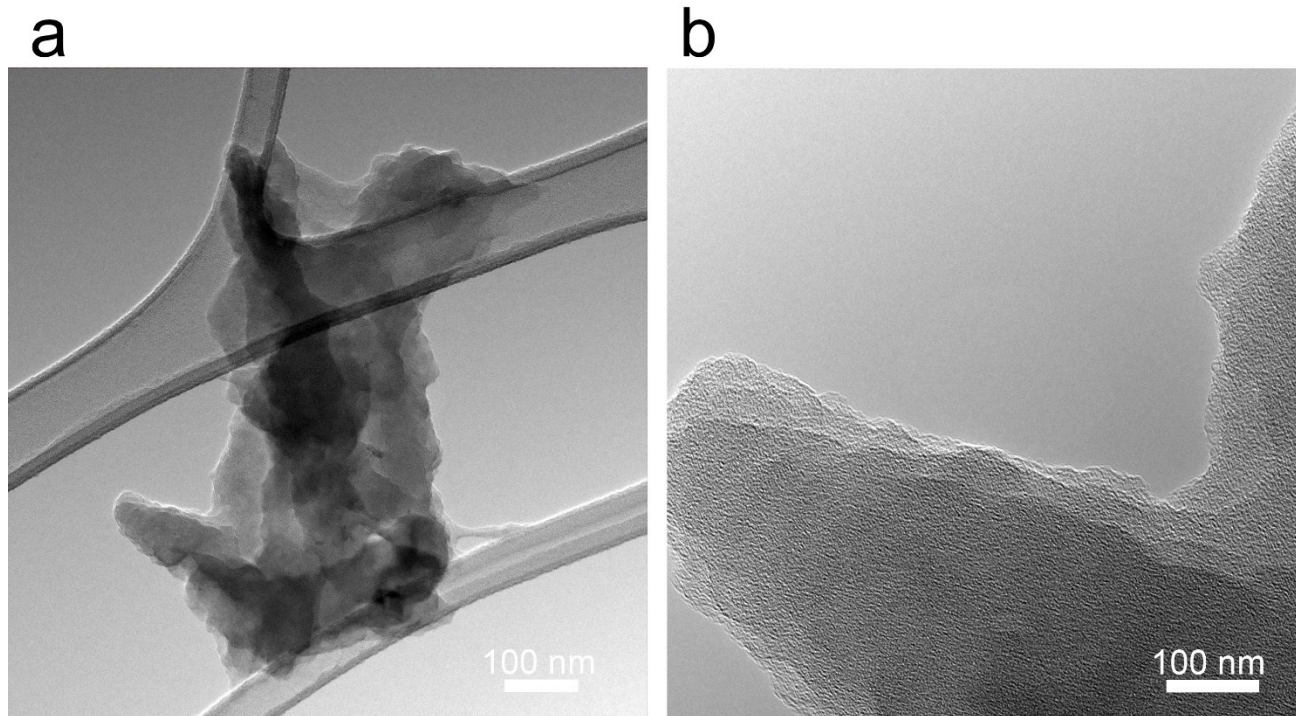
**Figure S2.** (a-b) Large-area and zoom-in TEM images of p-FePc.
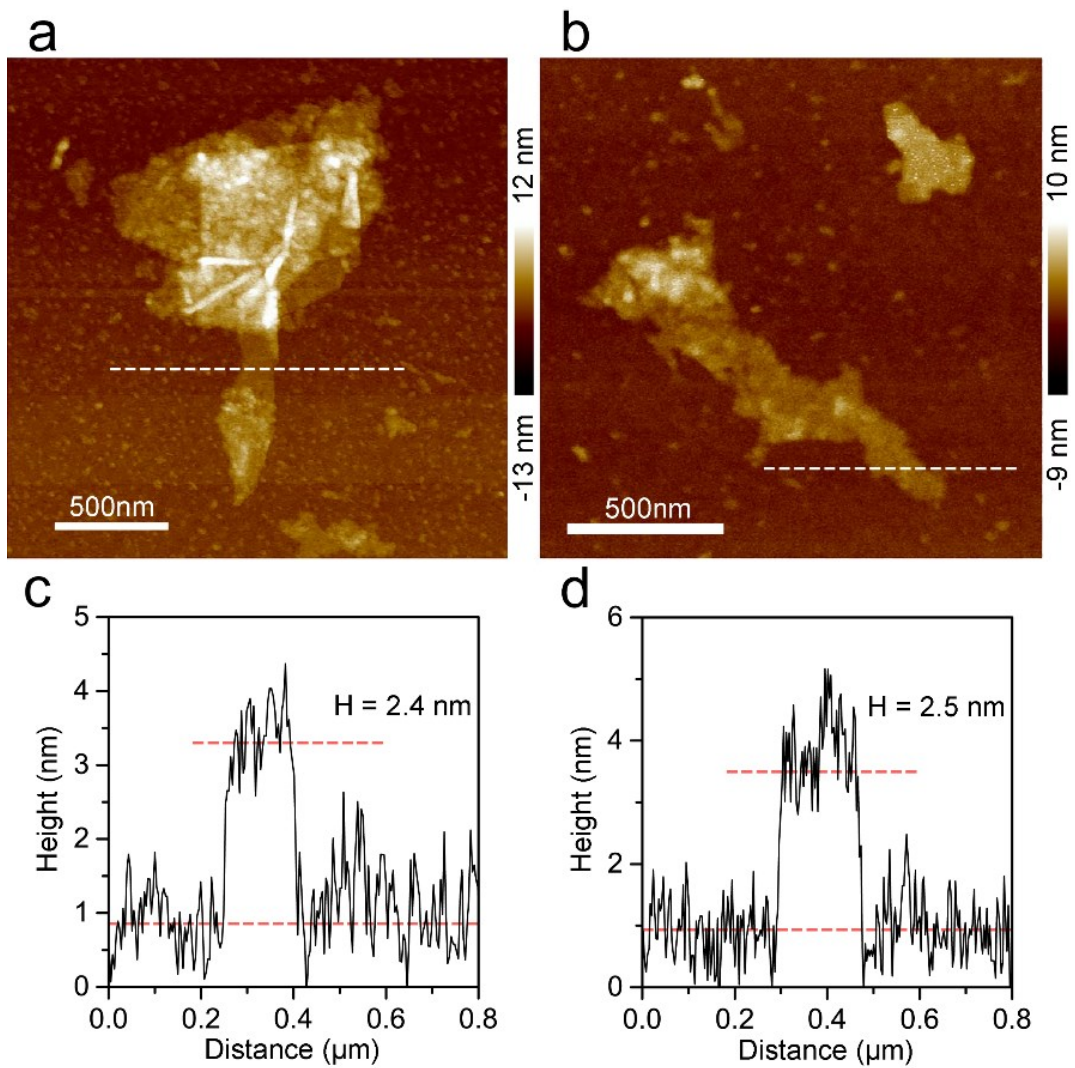
**Figure S3.** (a-b) AFM images of two representative p-FePc thin flakes. (c-d) The cross-sectional height profile along the dashed lines in a and b, respectively.
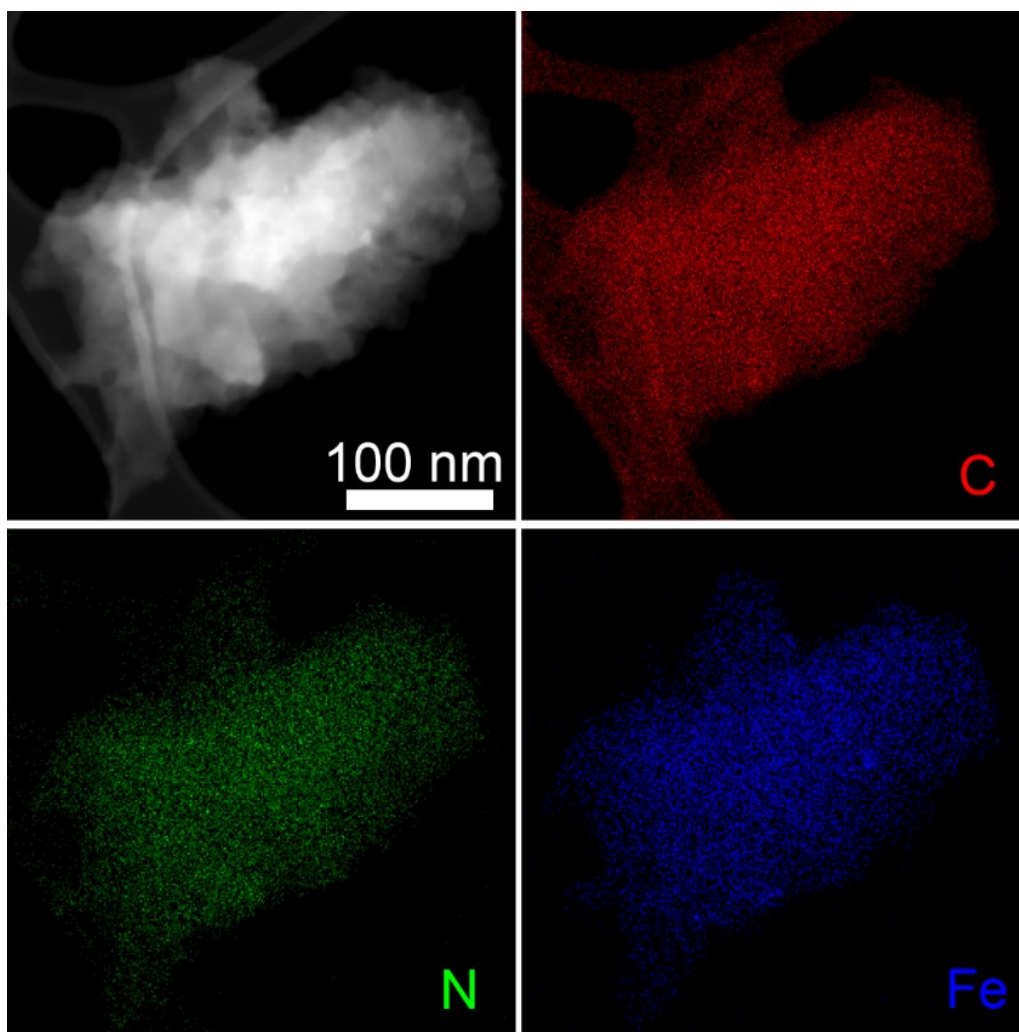
**Figure S4.** HAADF-STEM image of p-FePc and the corresponding EDS mapping images of C, N and Fe.
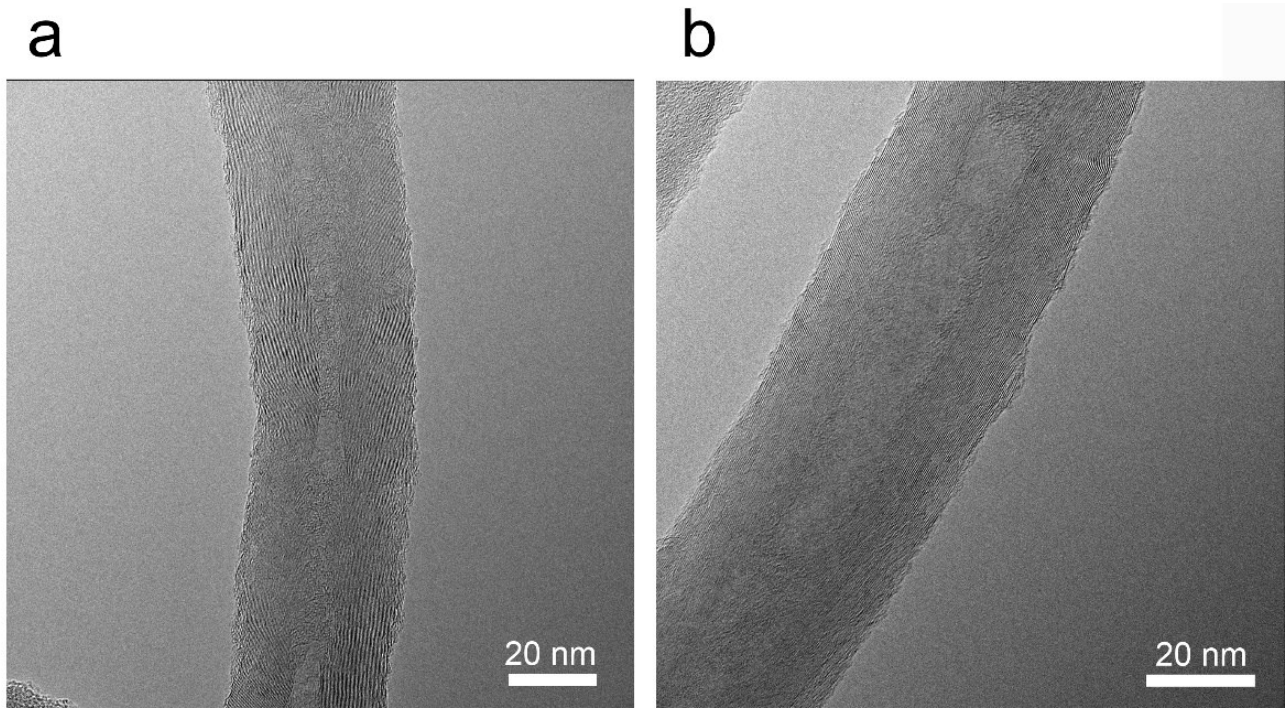
**Figure S5. (**a-b) High-resolution TEM images of CNTs used in this work.
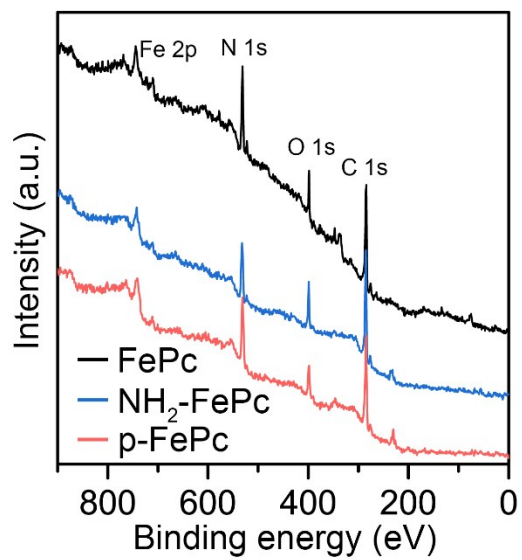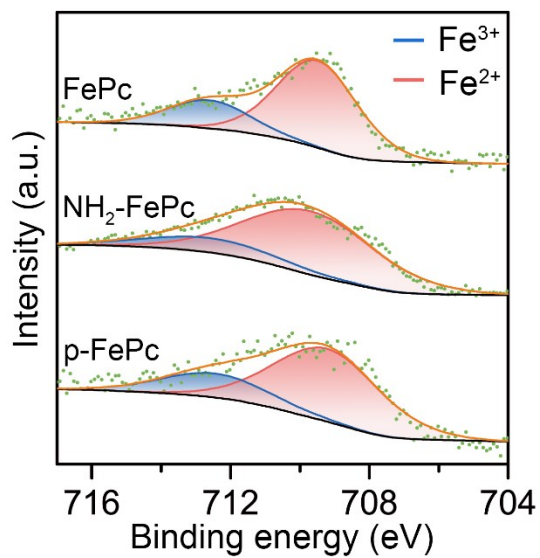
**Figure S6. (**a) Full XPS spectra of FePc, NH$_2$-FePc and p-FePc. (b) The corresponding high-resolution XPS Fe 2p spectra.
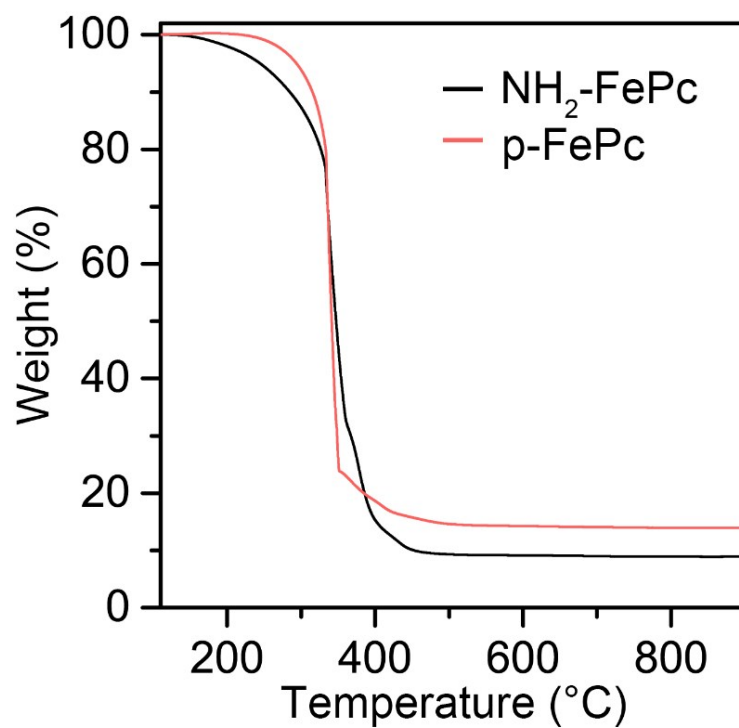
**Figure S7.** TGA curves of p-FePc and NH$_2$-FePc measured in air with a heating rate of 10 $^o$C/min.
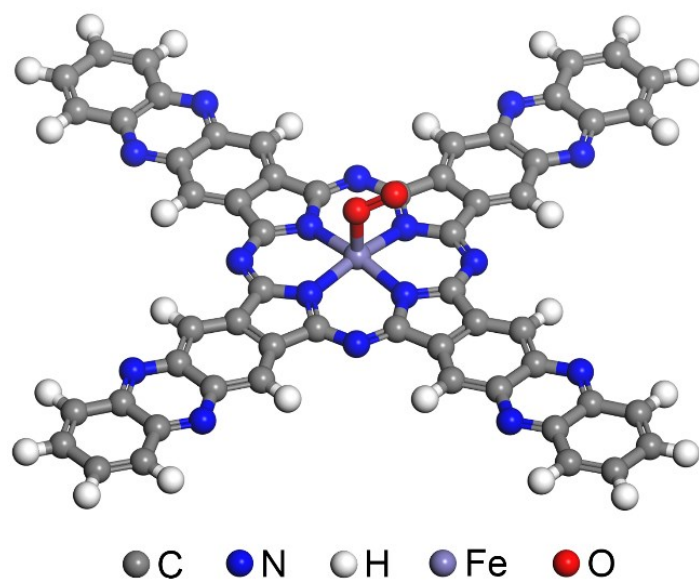
**Figure S8.** Proposed atomic structure of p-FePc used for fitting the experimental FT-EXAFS spectra.
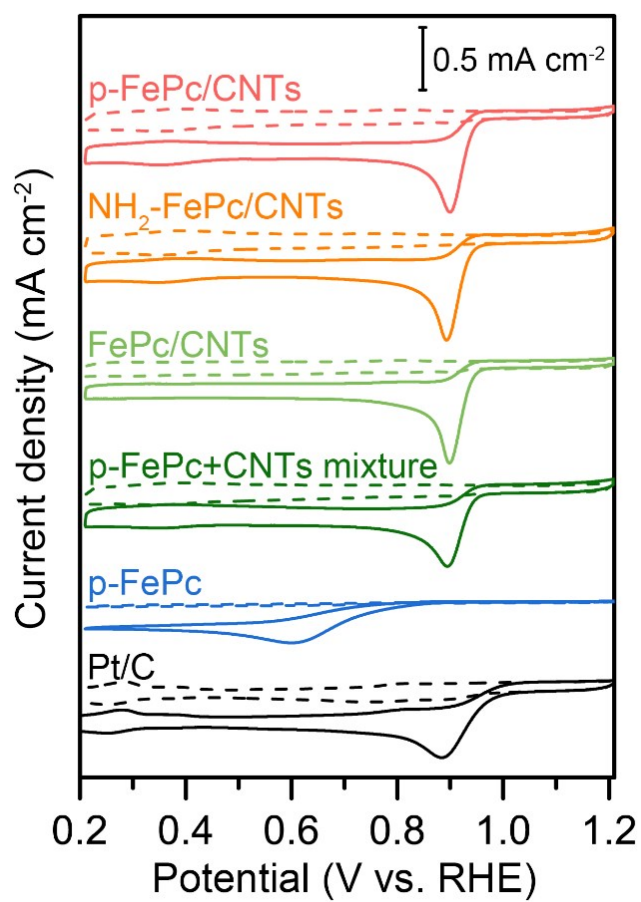
**Figure S9.** CV curves of the electrocatalysts in 0.1 M KOH saturated with $O_2$ (solid line) and $N_2$ (dash line).
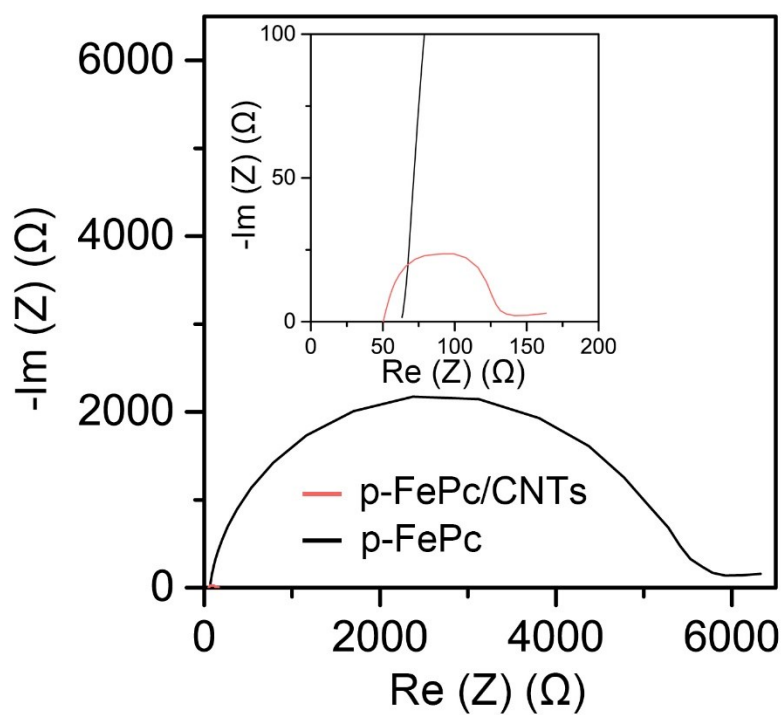
**Figure S10.** Nyquist plots of EIS over p-FePc/CNTs and pristine p-FePc catalysts in $O_2$-saturated 0.1M KOH with an inset of the enlarged Nyquist plots.
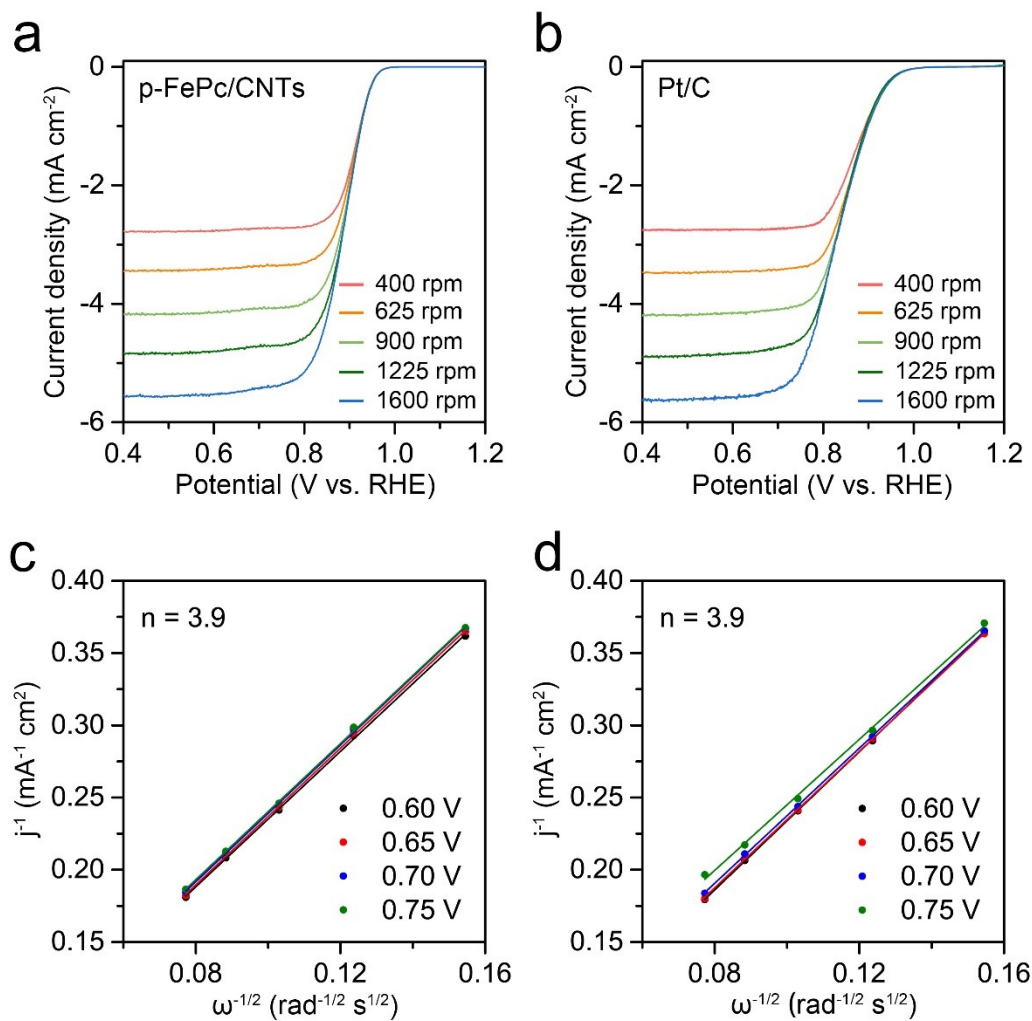
**Figure S11. (**a-b) LSV curves of (a) p-FePc/CNTs and (b) Pt/C in 0.1 M KOH at different rotation rates. (c-d) The corresponding Koutecky–Levich plots of p-FePc/CNTs and Pt/C at different potentials.
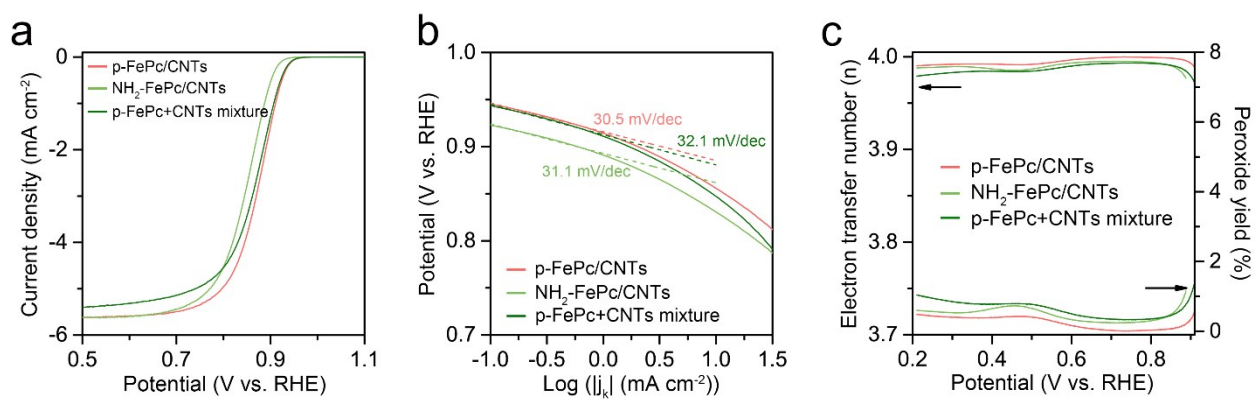
**Figure S12.** (a) LSV curves of p-FePc/CNTs, NH$_2$-FePc/CNTs and Pt/C in O$_2$-saturated 0.1 M KOH. (b) Tafel plots of p-FePc/CNTs, NH$_2$-FePc/CNTs and Pt/C. (c) Electron transfer number and peroxide yield of p-FePc/CNTs, NH$_2$-FePc/CNTs and Pt/C.
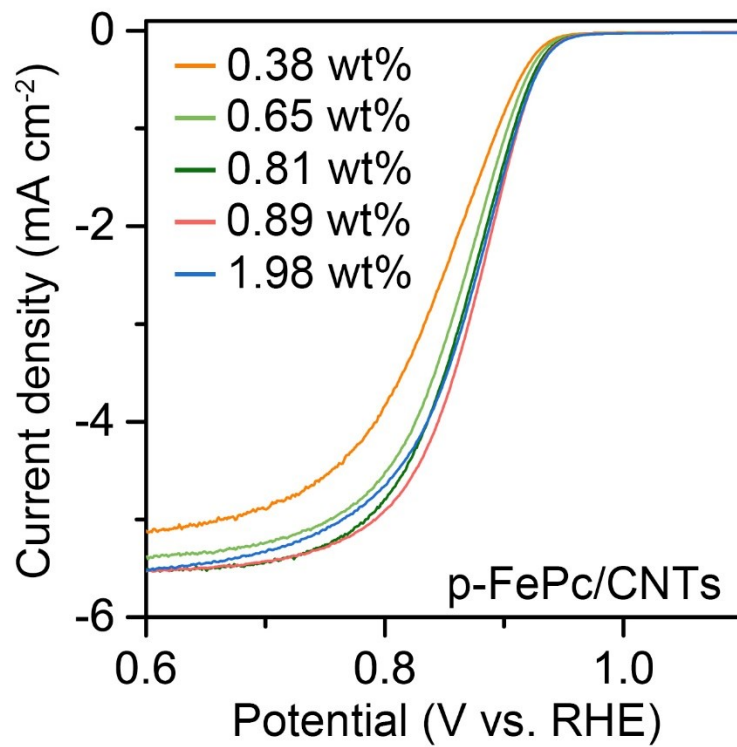
**Figure S13.** ORR polarization curves of p-FePc/CNTs with different Fe contents in 0.1 M KOH.
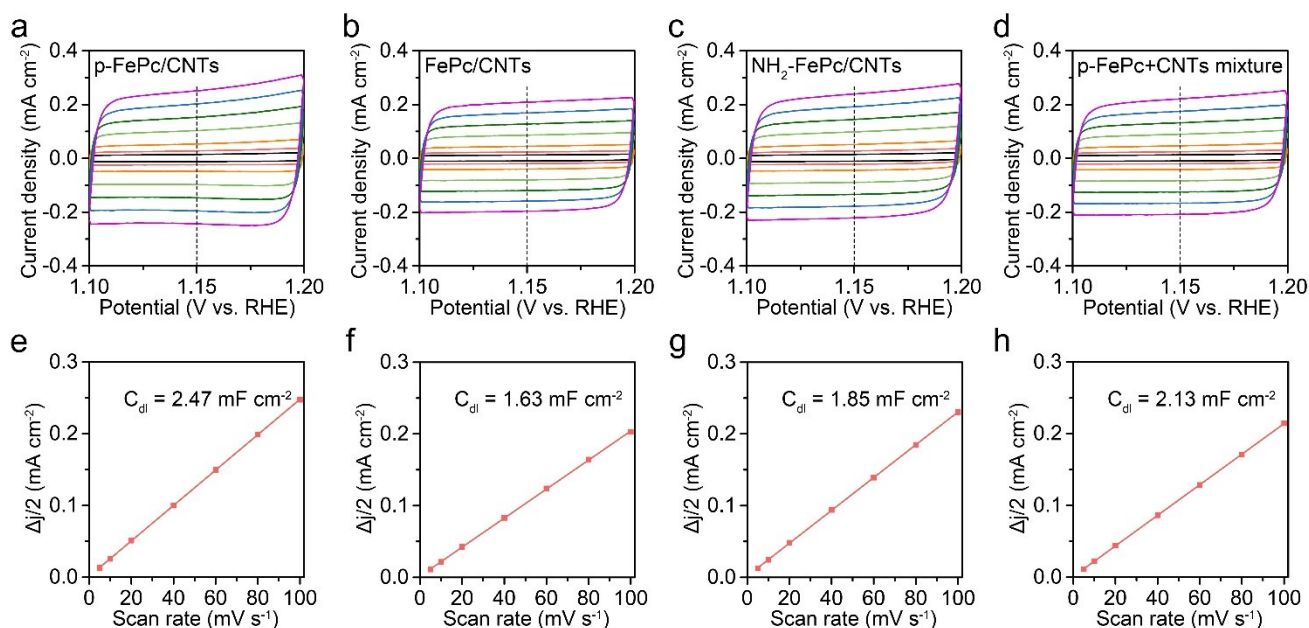
**Figure S14.** CV curves of (a) p-FePc/CNTs, (b) FePc/CNTs, (c) NH$_2$-FePc/CNTs and (d) p-FePc+CNTs mixture measured in a non-Faradaic region at the following scan rate: 5 mV s$^{-1}$ (black line), 10 mV s$^{-1}$ (red line), 20 mV s$^{-1}$ (orange line), 40 mV s$^{-1}$ (light green line), 60 mV s$^{-1}$ (green line), 80 mV s$^{-1}$ (blue line) and 100 mV s$^{-1}$ (purple line). The plots of $\Delta j/2$ at 1.15 V vs. RHE with different scan rate for (e) p-FePc/CNTs, (f) FePc/CNTs, (g) NH$_2$-FePc/CNTs and (h) p-FePc+CNTs mixture. The double-layer capacitance ($C_{dl}$) was estimated from the slope of the fitted line.
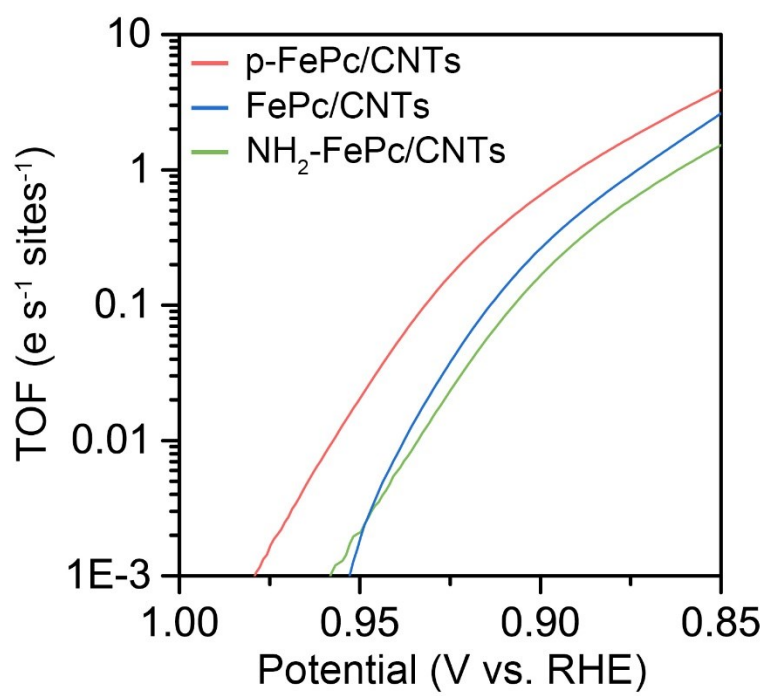
**Figure S15.** TOF determined from the measured current densities as a function of potential.
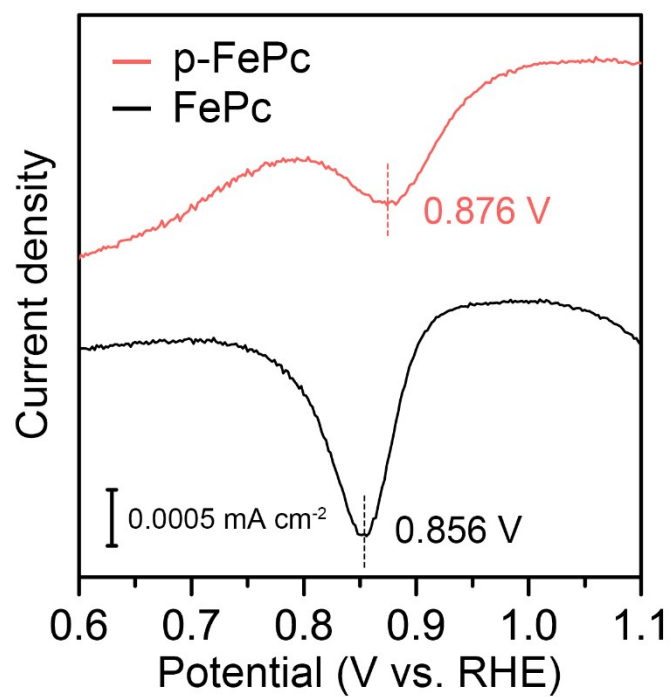
**Figure S16.** DPV curves of p-FePc and FePc measured in $N_2$-saturated 0.1 M KOH.

$$* + O_2 + H_2O + e^- \rightarrow *OOH + OH^- \qquad \text{step 1}$$

$$*OOH + e^- \rightarrow *O + OH^- \qquad \text{step 2}$$

$$*O + H_2O + e^- \rightarrow *OH + OH^- \qquad \text{step 3}$$

$$*OH + e^- \rightarrow * + OH^- \qquad \text{step 4}$$
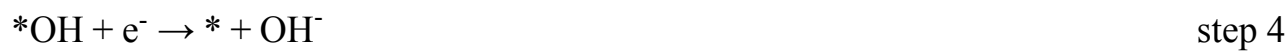
**Figure S17.** Four-step association mechanism of ORR in alkaline solution.
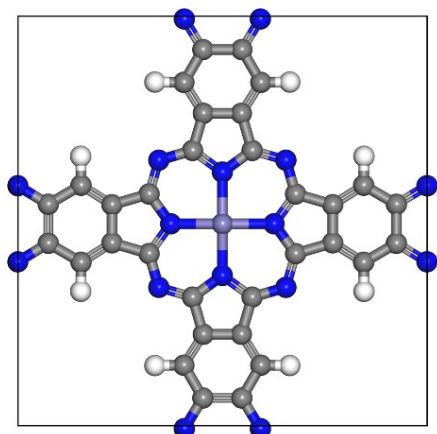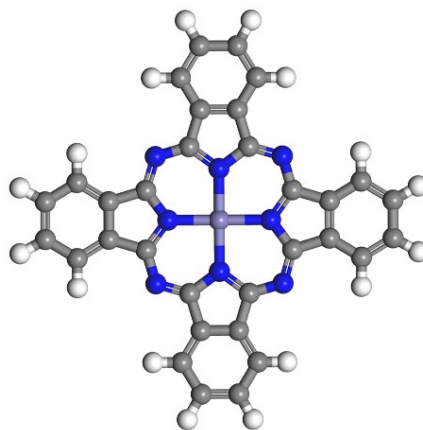
**Figure S18.** Optimized models of (a) the unit cell of p-FePc and (b) FePc.
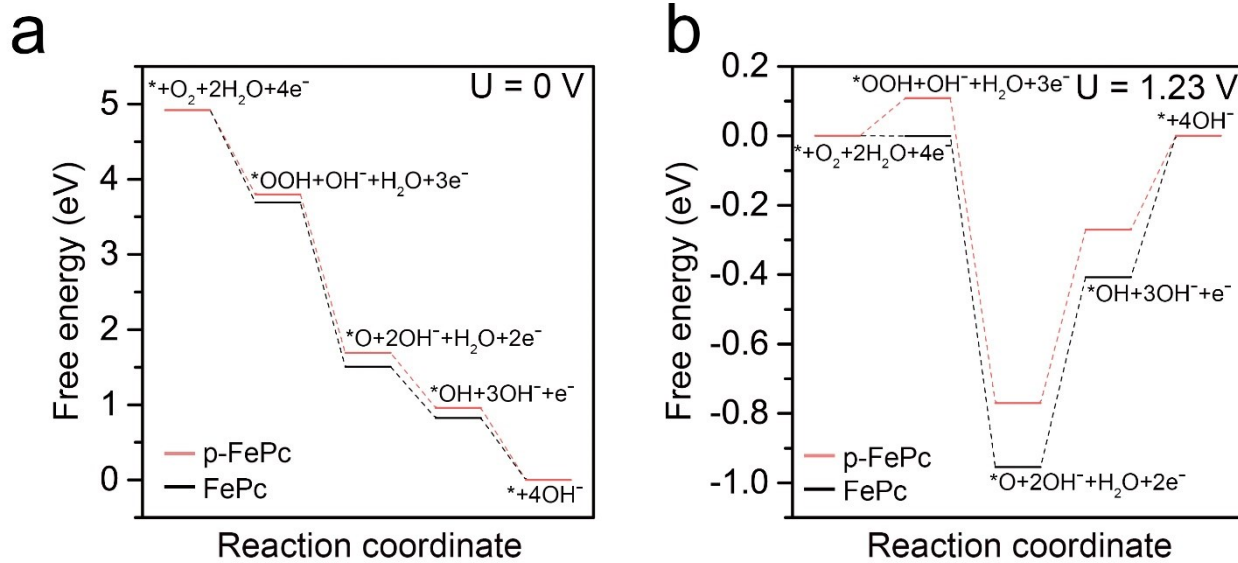
**Figure S19.** Free energy profile of oxygen reduction over p-FePc (red curve) and FePc (black curve) respectively at (a) U = 0 V and (b) U = 1.23 V.
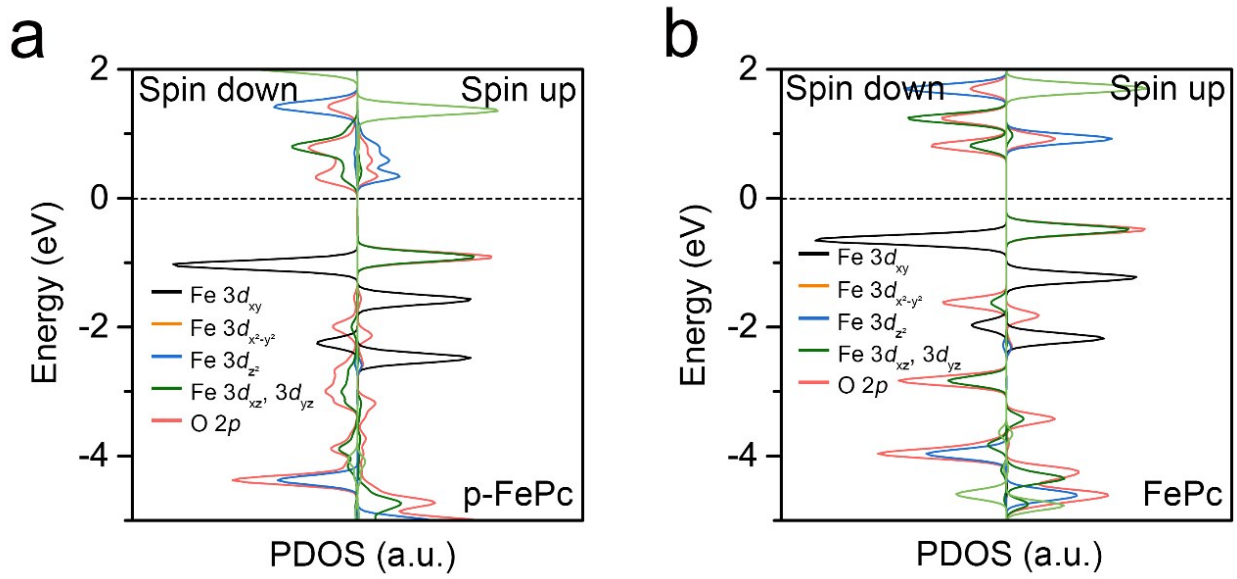
**Figure S20.** PDOS of Fe and adsorbed O in (a) O-p-FePc and (b) O-FePc.

|  | Fe content (wt%) | ECSA | TOF at 0.95 V ($e\ s^{-1}\ sites^{-1}$) | TOF at 0.90 V ($e\ s^{-1}\ sites^{-1}$) | TOF at 0.85V ($e\ s^{-1}\ sites^{-1}$) |
|---|---|---|---|---|---|
| p-FePc/CNTs | 0.89 | 61.8 | 0.0206 | 0.654 | 3.91 |
| FePc/CNTs | 0.80 | 40.8 | 0.0019 | 0.262 | 2.60 |
| $NH_2$-FePc/CNTs | 1.02 | 46.3 | 0.0021 | 0.165 | 1.52 |
| p-FePc+CNTs mixture | 0.95 | 53.3 | 0.0165 | 0.511 | 2.90 |

**Table S1.** Comparison of the Fe content, electrochemical surface area (ECSA) and estimated turnover frequencies (TOF) of the electrocatalysts.

| No. | Electrocatalysts | Half-wave potential (V vs. RHE) | Loading (mg cm$^{-2}$) | Reference |
|---|---|---|---|---|
| 1 | p-FePc/CNTs | 0.88 | 0.2 | This work |
| 2 | FePc/CNTs | 0.86 | 0.2 | This work |
| 3 | PcCu□O$_8$□Co/CNT | 0.83 | 0.48 | *Angew. Chem., Int. Ed.*, 2019, **58**, 10677–10682 |
| 4 | CAN□Pc(Fe/Co) | 0.84 | 0.1 | *Angew. Chem., Int. Ed.*, 2019, **58**, 14724–14730 |
| 5 | SA□Fe□HPC | 0.89 | 0.1 | *Angew. Chem., Int. Ed.*, 2018, **57**, 9038–9043 |
| 6 | Fe□N4 SAs/NPC | 0.885 | 0.4 | *Angew. Chem., Int. Ed.*, 2018, **57**, 8614–8618 |
| 7 | Pc-FePc/Mn-GCB | 0.90 | 0.2 | *Nano Energy*, 2017, **34**, 338–343 |
| 8 | FePc/Ti$_3$C$_2$T$_x$ | 0.886 | 0.25 | *Adv. Mater.*, 2018, **30**, 1803220 |
| 9 | Fe$_x$N/NGA | ~0.84 | 0.05 | *Adv. Funct. Mater.*, 2014, **24**, 2930–2937 |
| 10 | C-FePc(CN)$_8$/ZIF-8 | 0.91 | 0.2 | *ACS Catal.*, 2019, **9**, 6252–6261 |
| 11 | C-FePc/ZIF-8 | 0.88 | 0.2 | *ACS Catal.*, 2019, **9**, 6252–6261 |
| 12 | g-FePc | ~0.87 | 0.04 | *ACS Catal.*, 2013, **3**, 1263–1271 |
| 13 | CB@c-pFePc | ~0.88 | 0.15 | *ACS Appl. Mater. Interfaces*, 2018, **10**, 28664–28671 |
| 14 | CS-FePC$_{450}$ | 0.88 | 0.274 | *J. Mater. Chem. A*, 2019, **7**, 16690–16695 |
| 15 | FePcZnPor-CMP | 0.866 | 0.16 | *J. Mater. Chem. A*, 2018, **6**, 22851–22857 |
| 16 | Fe$_{0.5}$Co$_{0.5}$Pc-CP | 0.848 | 0.08 | *J. Mater. Chem. A*, 2018, **6**, 8349–8357 |
| 17 | MWCNT/FePc-SH | 0.864 | 0.3 | *J. Mater. Chem. A*, 2017, **5**, 1184–1191 |
| 18 | C-Z8Nc/FePc-900 | 0.885 | 0.4 | *J. Mater. Chem. A*, 2016, **4**, 7859–7868 |
| 19 | FePc/GS | 0.88 | 0.1 | *J. Mater. Chem. A*, 2015, **3**, 10013–10019 |
| 20 | FePc/CB-EC600 | 0.91 | 0.1 | *J. Mater. Chem. A*, 2015, **3**, 10013–10019 |

**Table S2.** Comparison of ORR performance of various phthalocyanine-based catalysts in 0.1 M KOH.

|  |  | ZPE (eV) | $E_{int}$ (eV) | T*S (eV) |
|---|---|---|---|---|
| p-FePc | *OOH | 0.427 | 0.097 | 0.197 |
|  | *O | 0.073 | 0.033 | 0.059 |
|  | *OH | 0.355 | 0.053 | 0.096 |
| FePc | *OOH | 0.408 | 0.060 | 0.118 |
|  | *O | 0.074 | 0.033 | 0.058 |
|  | *OH | 0.346 | 0.059 | 0.112 |

**Table S3.** Zero-point energy (ZPE) correction, internal energy contribution ($E_{int}$) and entropy contribution (S) to the Gibbs free energy of adsorbed chemical species (T = 298.15 K).

| Bond length | p-FePc | FePc | p-FePc-O | FePc-O |
|---|---|---|---|---|
| Fe-N1 (Å) | 1.927 | 1.930 | 1.960 | 1.955 |
| Fe-N2 (Å) | 1.927 | 1.930 | 1.960 | 1.955 |
| Fe-N3 (Å) | 1.928 | 1.931 | 1.960 | 1.955 |
| Fe-N4 (Å) | 1.928 | 1.931 | 1.960 | 1.955 |
| Fe-O (Å) | | | 1.641 | 1.642 |

**Table S4.** Geometrical parameters of the optimized configurations.

**References**

1. X. Zhang, Z. Wu, X. Zhang, L. Li, Y. Li, H. Xu, X. Li, X. Yu, Z. Zhang, Y. Liang and H. Wang, *Nat. Commun.*, 2017, **8**, 14675-146812.
2. Y. Du, Y. Zhu, S. Xi, P. Yang, H. O. Moser, M. B. H. Breese and A. Borgna, *J. Synchrotron Radiat.*, 2015, **22**, 839-843.
3. B. Ravel and M. Newville, *J. Synchrotron Radiat.*, 2005, **12**, 537-541.
4. Y. Liang, Y. Li, H. Wang, J. Zhou, J. Wang, T. Regier and H. Dai, *Nat. Mater.*, 2011, **10**, 780-786.
5. M. Wang, S. Liu, T. Qian, J. Liu, J. Zhou, H. Ji, J. Xiong, J. Zhong and C. Yan, *Nat. Commun.*, 2019, **10**, 341.
6. X. Ao, W. Zhang, Z. Li, J.-G. Li, L. Soule, X. Huang, W.-H. Chiang, H. M. Chen, C. Wang, M. Liu and X. C. Zeng, *ACS Nano*, 2019, **13**, 11853-11862.
7. U. I. Kramm, I. Herrmann-Geppert, J. Behrends, K. Lips, S. Fiechter and P. Bogdanoff, *J. Am. Chem. Soc.*, 2016, **138**, 635-640.
8. J. Li, S. Ghoshal, W. Liang, M.-T. Sougrati, F. Jaouen, B. Halevi, S. McKinney, G. McCool, C. Ma, X. Yuan, Z.-F. Ma, S. Mukerjee and Q. Jia, *Energy Environ. Sci.*, 2016, **9**, 2418-2432.
9. M. Zeng, Y. Liu, F. Zhao, K. Nie, N. Han, X. Wang, W. Huang, X. Song, J. Zhong and Y. Li, *Adv. Funct. Mater.*, 2016, **26**, 4397-4404.
10. Y. Liu, F. Chen, W. Ye, M. Zeng, N. Han, F. Zhao, X. Wang and Y. Li, *Adv. Funct. Mater.*, 2017, **27**, 1606034.
11. T. Wang, J. Wu, Y. Liu, X. Cui, P. Ding, J. Deng, C. Zha, E. Coy and Y. Li, *Energy Storage Mater.*, 2019, **16**, 24-30.
12. G. Kresse and J. Hafner, *Phys. Rev. B*, 1993, **48**, 13115-13118.
13. G. Kresse and J. Hafner, *Phys. Rev. B*, 1994, **49**, 14251-14269.
14. G. Kresse and D. Joubert, *Phys. Rev. B*, 1999, **59**, 1758-1775.
15. P. E. Blöchl, *Phys. Rev. B*, 1994, **50**, 17953-17979.
16. J. P. Perdew, K. Burke and M. Ernzerhof, *Phys. Rev. Lett.*, 1996, **77**, 3865-3868.
17. X.-M. Cao, R. Burch, C. Hardacre and P. Hu, *Catal. Today*, 2011, **165**, 71-79.
18. G. W. T. M. J. Frisch, H. B. Schlegel, G. E. Scuseria, M. A. Robb, J. R. Cheeseman, G. Scalmani, V. Barone, B. Mennucci, G. A. Petersson, H. Nakatsuji, M. Caricato, X. Li, H. P. Hratchian, A. F. Izmaylov, J. Bloino, G. Zheng, J. L. Sonnenberg, M. Hada, M. Ehara, K. Toyota, R. Fukuda, J. Hasegawa, M. Ishida, T. Nakajima, Y. Honda, O. Kitao, H. Nakai, T. Vreven, J. A. Montgomery,

Jr., J. E. Peralta, F. Ogliaro, M. Bearpark, J. J. Heyd, E. Brothers, K. N. Kudin, V. N. Staroverov, R. Kobayashi, J. Normand, K. Raghavachari, A. Rendell, J. C. Burant, S. S. Iyengar, J. Tomasi, M. Cossi, N. Rega, J. M. Millam, M. Klene, J. E. Knox, J. B. Cross, V. Bakken, C. Adamo, J. Jaramillo, R. Gomperts, R. E. Stratmann, O. Yazyev, A. J. Austin, R. Cammi, C. Pomelli, J. W. Ochterski, R. L. Martin, K. Morokuma, V. G. Zakrzewski, G. A. Voth, P. Salvador, J. J. Dannenberg, S. Dapprich, A. D. Daniels, O. Farkas, J. B. Foresman, J. V. Ortiz, J. Cioslowski, and D. J. Fox, Gaussian 09 (Revision A.02), Gaussian, Inc., Wallingford CT, 2009.

19. C. Lee, W. Yang and R. G. Parr, *Phys. Rev. B*, 1988, **37**, 785-789.

20. A. D. Becke, *J. Chem. Phys.*, 1993, **98**, 5648-5652.

21. I. C. Man, H.-Y. Su, F. Calle-Vallejo, H. A. Hansen, J. I. Martínez, N. G. Inoglu, J. Kitchin, T. F. Jaramillo, J. K. Nørskov and J. Rossmeisl, *ChemCatChem*, 2011, **3**, 1159-1165.

22. R. Dronskowski and P. E. Bloechl, *J. Phys. Chem. A*, 1993, **97**, 8617-8624.

23. V. L. Deringer, A. L. Tchougréeff and R. Dronskowski, *J. Phys. Chem. A*, 2011, **115**, 5461-5466.

24. S. Maintz, V. L. Deringer, A. L. Tchougréeff and R. Dronskowski, *J. Comput. Chem.*, 2013, **34**, 2557-2567.

25. S. Maintz, V. L. Deringer, A. L. Tchougréeff and R. Dronskowski, *J. Comput. Chem.*, 2016, **37**, 1030-1035.